数理解析研究所講究録
第92巻 1970年 62-84

THREE-DIMENSIONAL FEATURES OF THERMAL CONVECTION IN A PLANE COUETTE FLOW

Tomio Asai
Geophysical Institute, Kyoto University

1. Introduction

Jeffreys (1928) suggested that a constant shear flow in an unstably stratified fluid stabilizes all modes of perturbations in a vertical plane parallel to the flow except for one mode of infinite wavelength. Then he conjectured that convective disturbance occurs in strips instead of in the symmetrical Bènard cells. His conjecture was supported by laboratory experiments on thermal convection in a shear flow performed by Terada (1928), Graham (1934) and Chandra (1938). A theoretical study of hydrodynamic stability of a stratified plane Couette flow has been made by Taylor (1931), Case (1960), Dyson (1960), Riis (1962) and others. They concluded that a stably stratified Couette flow is hydrodynamically stable. Kuo (1963) extended the theory to a plane Couette flow in an unstably stratified fluid layer and proved Jeffreys' conjecture. Based on perturbation analysis, Kuo concluded that the preferred mode of perturbation is roll-type convection parallel to the basic flow.

Asai (1964) made a numerical experiment on thermal convection in a shear flow and discussed the dynamical structure of convection and the related energy conversion. Asai showed that the axis of convection cells tilts toward the shear with height. This results in the interaction between the convective motion and the basic flow which transforms the kinetic energy of convection into that of the basic flow through upward transport of horizontal momentum against vertical shear, i.e., counter-gradient momentum transport. Thus, vertical shear tends to suppress development of convection in a vertical plane parallel to the basic flow.

Moreover, the discrepancy which develops between the central axes of an ascending region and of a warm region of convection reduces the conversion of potential to kinetic energy which is a principal cause of the development of convection. This result is, however, restricted to two-dimensional convection along the basic flow. In contrast to the predominantly one-way flow of energy toward higher wavenumber in three-dimensional turbulence, energy is cascaded toward lower wavenumbers in two-dimensional turbulence (e.g., Lilly, 1969). The tendency to convert perturbation kinetic energy into mean flow kinetic energy may be regarded as an example of a general result of two-dimensional turbulence. Therefore, we cannot rule out the possibility that the conclusion obtained above might be peculiar to a two-dimensional convection. In dealing with three-dimensional convection in a nonlinear hydrodynamic system, we shall still encounter some practical difficulties. A perturbation analysis of a three-dimensional convection is useful because it affords an insight into the dynamical processes involved in a thermal convection in a shear flow.

Recently, Deardorff (1965), Gallagher and Mercer (1965), Ingersoll (1966) and Asai and Nakasuji (1968) analyzed the full sixth-order stability problem numerically instead of Kuo's incomplete treatment on diffusion terms. Then they showed neutral stability curve for various ranges of some physical parameters such as Rayleigh number, Reynolds number, Prandtl number and horizontal wavenumber of a perturbation. In this paper we will extend the previous papers (Asai and Nakasuji, 1968) by examining in detail the structure of the unstable perturbation and the associated energy conversion.

2. Basic equations

Consider a horizontal fluid layer which is bounded above and below by horizontal planes at z = 0 and z = h, respectively (see Fig. 1). The coordinate axes x and y lie in a horizontal plane, while z is the vertical axis. In the undisturbed condition, the distributions of temperature and velocity in the fluid depend linearly on z, i.e.,

$$\bar{u} = u_o + \Lambda z \tag{2.1}$$

$$\bar{T} = T_o - \Gamma z \tag{2.2}$$

where $\Gamma(\equiv -\partial\bar{T}/\partial z)$ is the constant lapse rate of the temperature and $\Lambda(\equiv \partial\bar{u}/\partial z)$ is the constant vertical shear of the basic flow which is taken to be parallel to the x axis. T_o and u_o are the temperature and the velocity at z = 0. The relationship between temperature $\bar{T}$ and density $\bar{\rho}$ is expressed by

$$\bar{\rho} = \rho_o \{1 - \alpha (\bar{T} - T_o)\} \tag{2.3}$$

where α is the thermal expansion coefficient and ρ_o is the density at z = 0. The pressure $\bar{p}$ can be derived from the hydrostatic equation

$$\frac{\partial \bar{p}}{\partial z} = -g\bar{\rho} \tag{2.4}$$

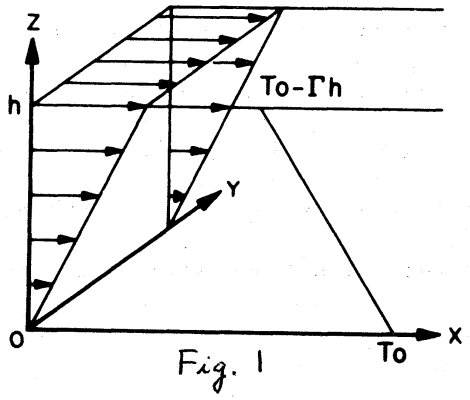

Fig. 1

where g is the acceleration due to gravitational force.

The linearized equations governing small amplitude perturbation motions under a Boussinesq approximation may be written as follows:

$$\frac{\partial u'}{\partial t} + \bar{u}\frac{\partial u'}{\partial x} + w'\frac{\partial \bar{u}}{\partial z} = -\frac{1}{\rho_o}\frac{\partial p'}{\partial x} + \nu \nabla^2 u' \tag{2.5}$$

$$\frac{\partial v'}{\partial t} + \bar{u}\frac{\partial v'}{\partial x} = -\frac{1}{\rho_o}\frac{\partial p'}{\partial y} + \nu \nabla^2 v' \tag{2.6}$$

$$\frac{\partial w'}{\partial t} + \bar{u}\frac{\partial w'}{\partial x} = -\frac{1}{\rho_o}\frac{\partial p'}{\partial z} + g\alpha T' + \nu \nabla^2 w' \tag{2.7}$$

$$\frac{\partial u'}{\partial x} + \frac{\partial v'}{\partial y} + \frac{\partial w'}{\partial z} = 0 \tag{2.8}$$

$$\frac{\partial T'}{\partial t} + \bar{u}\frac{\partial T'}{\partial x} + w'\frac{\partial \bar{T}}{\partial z} = \kappa \nabla^2 T' \tag{2.9}$$

where u', v', w', T' and p' are the velocity components in the x, y, and z directions, the temperature and the pressure of a perturbation,

respectively, ν is the coefficient of kinematic viscosity, $\varkappa$ is the coefficient of thermometric conductivity, and ∇^2 denotes the three-dimensional Laplacian operator.

Eliminating u', v', and p' from (2.5) to (2.8), we can reduce (2.5) to (2.9) to the following two equations for w' and T':

$$\left(\frac{\partial}{\partial t} + \bar{u}\,\frac{\partial}{\partial x} - \nu\,\nabla^2\right)\nabla^2 w' - g\alpha\nabla_H^2\,T' = 0 \tag{2.10}$$

$$\left(\frac{\partial}{\partial t} + \bar{u}\,\frac{\partial}{\partial x} - \varkappa\,\nabla^2\right)T' - \Gamma\,w' = 0 \tag{2.11}$$

where

$$\nabla_H^2 \equiv \frac{\partial^2}{\partial x^2} + \frac{\partial^2}{\partial y^2}$$

On the other hand, differentiating (2.5) with respect to y, (2.6) with respect to x, and taking the difference, we can derive the equation for the vertical component of vorticity:

$$\frac{\partial \zeta'}{\partial t} + \bar{u}\,\frac{\partial \zeta'}{\partial x} - \Lambda\,\frac{\partial w'}{\partial y} = \nu\,\nabla^2\,\zeta' \tag{2.12}$$

where

$$\zeta' \equiv \frac{\partial v'}{\partial x} - \frac{\partial u'}{\partial y} \tag{2.13}$$

Since we can write

$$\nabla_H^2 u' = -\frac{\partial \zeta'}{\partial y} - \frac{\partial^2 w'}{\partial x \partial z} \tag{2.14}$$

and

$$\nabla_H^2 v' = \frac{\partial \zeta'}{\partial x} - \frac{\partial^2 w'}{\partial y \partial z} \tag{2.15}$$

with the aid of (2.8) and (2.13), the horizontal component of motion can also be obtained.

3. Boundary conditions

We assume both the upper and lower boundary surfaces are fixed and smooth. This means that both the normal components of velocity and the tangential stresses must vanish at the boundaries, i.e.,

$$w' = \frac{\partial^2 w'}{\partial z^2} = \frac{\partial \zeta'}{\partial z} = 0 \qquad \text{at } z = 0 \text{ and } h \tag{3.1}$$

with the aid of (2.8) and (2.13).

Furthermore, the constant temperatures are assumed to be maintained at both the upper and lower boundaries, respectively:

$$T' = 0 \qquad \text{at } z = 0 \text{ and } h \tag{3.2}$$

4. Formulation of the problem

Now we take solutions of the form

$$\begin{pmatrix} w' \\ T' \\ \zeta' \\ u' \\ v' \end{pmatrix} = \begin{pmatrix} w\,(z) \\ \Theta\,(z) \\ Z\,(z) \\ U\,(z) \\ V\,(z) \end{pmatrix} \exp\{i\,(k_x\,x + k_y y) + \sigma t\} \tag{4.1}$$

where k_x and k_y are the wavenumbers in the x and y directions, respectively. A real part of the frequency σ denotes an amplification rate. Let us define the following dimensionless quantities denoted by the superscript *:

$$\left.\begin{aligned} &\sigma = \sigma^* \nu\, h^{-2} \\ &k_x = k_x^*\, h^{-1},\ k_y = k_y^*\, h^{-1},\quad z = z^*\, h \\ &U = U^*\, \nu\, h^{-1},\quad V = V^*\, \nu\, h^{-1},\quad W = W^*\, \nu\, h^{-1} \\ &\overline{u} = \overline{u}^*\, \Lambda\, h \\ &Z = Z^*\, \Lambda \\ &\Theta = \Theta^*\, \Gamma\, h \end{aligned}\right\} \tag{4.2}$$

Substituting (4.1) into (2.10), (2.11), (2.12), (2.14), and (2.15) and using (4.2), we obtain

$$\{\sigma^* + iR_e k_x^* z^* - (\frac{d^2}{dz^{*2}} - k^{*2})\} (\frac{d^2}{dz^{*2}} - k^{*2}) W^* + P_r^{-1} R_a k^{*2} \Theta^* = 0 \tag{4.3}$$

$$\{\sigma^* + iR_e k_x^* z^* - P_r^{-1} (\frac{d^2}{dz^{*2}} - k^{*2})\} \Theta^* - W^* = 0 \tag{4.4}$$

$$\{\sigma^* + iR_e k_x^* z^* - (\frac{d^2}{dz^{*2}} - k^{*2})\} Z^* - ik_y^* W^* = 0 \tag{4.5}$$

$$U^* = ik^{*-2} (k_x^* \frac{dW^*}{dz^*} + R_e k_y^* Z^*) \tag{4.6}$$

$$V^* = ik^{*-2} (k_y^* \frac{dW^*}{dz^*} - R_e k_x^* Z^*) \tag{4.7}$$

where $k^{*2} \equiv k_x^{*2} + k_y^{*2}$, $P_r \equiv \nu/\varkappa$ (Prandtl number), $R_a \equiv g\alpha\Gamma h^4/\varkappa\nu$ (Rayleigh number), and $R_e \equiv \Lambda h^2/\nu$ (Reynolds number). In deriving the above equations, we used the relationship $\bar{u}^* = z^*$, which can be obtained assuming $u_o = 0$. The Richardson number $R_i \equiv g\alpha\Gamma/\Lambda^2$ will be adopted instead of R_e, which is related to the other dimensionless parameters in the form $R_e = \{R_a/(P_r R_i)\}^{\frac{1}{2}}$. Note that R_i defined here has a sign opposite from that customarily used.

Dimensionless forms corresponding to the boundary conditions (3.1) and (3.2) are

$$W^* = \frac{d^2W^*}{dz^{*2}} = \frac{dZ^*}{dz^*} = 0 \qquad \text{at } z^* = 0 \text{ and } 1 \tag{4.8}$$

$$\Theta^* = 0 \qquad \text{at } z^* = 0 \text{ and } 1 \tag{4.9}$$

5. Numerical procedure

The system of ordinary differential equations (4.3) and (4.4) is transformed to a set of algebraic equations by approximating the derivatives of W^* and Θ^* with respect to z^* by finite differences. A frequency equation is then derived under the condition of a nonzero value for W^* and Θ^*. Asai and Nakasuji (1968) showed that a solution of good accuracy would be obtained using a rather small number of grid points in the layer, in particular, for a perturbation of the lowest mode in the vertical which would be of primary interest here.

In the present paper, we will proceed to a further calculation to solve the eigenvectors W^* and Θ^* for each eigenvalue σ^*. Then Z^* can be obtained by solving (4.5) and U^* and V^* can be determined from (4.6) and (4.7). The numerical method to solve (4.3) to (4.7) is summarized in the Appendix.

Using the solution obtained above, we can investigate the structure of perturbations and the related energy conversion processes, as well as stability characteristics. In the following, the Prandtl number, P_r, is assumed to be 7 which is nearly equal to the one for water at s.t.p. A 16-layer representation is used for the numerical calculation, unless specifically stated otherwise (see Appendix).

6. Stability characteristics and structure of unstable perturbations

First, the amplification rate of unstable perturbations will be examined for different values of some parameters relevant to stability properties. Figure 2 shows the amplification rate as a function of the Richardson number R_i and the dimensionless vectorial horizontal wavenumber of the perturbation k^*. Another representation of stability characteristics is made in Fig. 3 in which variations of the amplification rate with k^* are shown for different values of R_i. Both are for the case of $R_a = 10^5$ and $k_x^* = k_y^*$. As seen in Figs. 2 and 3, there is a preferred perturbation for which the amplification rate attains a maximum for a given value of R_i and the preferred perturbation shifts its wavenumber slightly toward a larger value with an increase of R_i. The neutral curve, at which the amplification rate is zero, shows two cut-off ends of instability, one at a small wavenumber and the other at a large wavenumber. As the value of R_i increases, the amplification rate increases and tends to approach the one for $R_i = 10^5$ which actually may be regarded as the case of no shear. On the other hand, no unstable perturbation exists when R_i is smaller than a certain critical value. It is evident that the shear of the basic flow exerts an influence on reducing development of a perturbation. The stability characteristics described above are quite similar to those obtained for the smaller value of R_a (Asai and Nakasuji, 1968).

It is, however, worth mentioning that the instability domain in Figs. 2 and 3 can be divided into two portions having different characteristics, as indicated by the dotted line. One is the region of longer waves in which a preferred perturbation exists, and the other is the region of shorter waves in which the variation of amplification rate with wavenumber is relatively small. The characteristic difference between the two types is shown more clearly in Fig. 4 which illustrates the phase velocity of an unstable perturbation as a function of wavenumber for different values of R_i. The ordinate indicates the phase velocity of an unstable perturbation c relative to the basic flow velocity at the midlevel $\bar{u}_{\frac{1}{2}}$. Here $c = -\sigma_i/k_x$, and σ_i denotes an imaginary part of σ. While the longer unstable perturbation moves at the velocity $\bar{u}_{\frac{1}{2}}$, the shorter unstable perturbations consisting of two solutions propagate at the same speed in the opposite direction relative to the basic flow at the midlevel. Following Kuo (1963), the longer unstable perturbation is hereafter referred to as a stationary unstable perturbation and the shorter ones are called transitive unstable perturbations. When the thermal stratification is less unstable (in other words the Rayleigh number is smaller), the transitive unstable perturbations vanish.

As shown in Fig. 3, one or more other stationary unstable waves may appear as R_i increases. They are characterized by a smaller ampli-

fication rate and a higher mode in the vertical. They seem to be insignificant for the present linear stability theory because the most unstable perturbation of the lowest mode is of primary importance.

We now examine the structures of both the stationary and the transitive unstable perturbations. Figures 5(a) and (b) show distributions of vertical velocities and temperatures of two types of perturbations in a vertical plane parallel to the basic flow, respectively, for the case of $R_a = 10^5$ and $R_i = 1$: (a) is the stationary unstable perturbation for $k_x^* = k_y^* = 1$ ($k^* = \sqrt{2}$), which is nearly a preferred mode, and (b) is a transitive unstable perturbation for $k_x^* = k_y^* = 3$ ($k^* = 3\sqrt{2}$). The ordinate indicates the dimensionless height, and the abscissa indicates the phase angle in the x direction. Contours of vertical velocity and temperature are shown by solid and broken lines, respectively. A central axis of ascending motion, denoted by a thick solid line, tilts with height in the direction of the basic flow. The tilt of an axis of warm air is large compared with that of the ascending motion. Nevertheless, the warm core coincides with maximum ascending motion and the cold core with maximum descending motion. As far as these features of unstable perturbation are concerned, there is no significant difference between the present linear theory and the nonlinear numerical experiment (Asai, 1964).

For the stationary perturbation, ascending warm cores, as well as descending cold cores, are located at the midlevel

but for the transitive perturbation the locations of the cores are different. These circumstances are clearly illustrated in Figs. 6(a) and (b) which show vertical distributions of vertical velocities and temperatures for both perturbations. The vertical profile of the amplitude of vertical velocity and that of temperature are asymmetric about the midlevel for the transitive perturbation. The maximum amplitude is located lower than the midlevel. The other of a set of two transitive perturbations not shown here is exactly symmetrical about the midlevel with the one shown here. The "steering level," denoted by an arrow, at which the basic flow is coincident with the phase velocity of a perturbation, is also at the level of maximum amplitude for the transitive perturbation.

Figures 7(a) and (b) show vertical profiles of vertical transports of heat and horizontal momentum (u) by solid and broken lines, respectively. As could be expected from the structure described above, we can observe upward heat transport at every level for the stationary unstable perturbation and mainly in lower levels for the transitive unstable perturbation (see Fig. 7). Averaged over the whole layer, both the perturbations transport heat upward and transform potential energy into kinetic energy of the perturbations. The downward transfer of momentum is shown for each case. This is opposite from the result obtained by Asai (1964) in the numerical experiment for a two-dimensional convection parallel to the basic flow. The momentum transfer and the related properties of perturbations will be discussed in the next section.

7. Vertical momentum transfer and energy conversion

Let us describe the energy conversion mechanism of the problem. The equation for kinetic energy of perturbations can be derived from (2.5), (2.6), and (2.7) by making use of (2.8) and (3.1) as follows:

$$\frac{\partial}{\partial t}\langle K' \rangle = g\alpha\langle T'w' \rangle - \Lambda \langle u'w' \rangle - \nu \langle \xi'^2 + \eta'^2 + \zeta'^2 \rangle \qquad (7.1)$$

where K' is the kinetic energy of perturbation which is defined as $K' = \frac{1}{2}(u'^2 + v'^2 + w'^2)$ and ξ', η' and ζ' are the x, y, and z components of perturbation vorticity, respectively. Angular brackets $\langle\ \rangle$ denote an average over a volume bounded by the planes $z = 0$ and $z = h$ and by one wavelength in the x and y directions respectively. Let us define kinetic energy of the mean flow $\bar{K}$ and potential energy P as follows:

$$\bar{K} = \tfrac{1}{2}\bar{u}^2 \qquad \text{and} \qquad P = -g\alpha z\bar{T}$$

The first term of the right-hand side of (7.1), $g\alpha \langle T'w' \rangle$, indicates the conversion between the potential energy and the kinetic energy of perturbation, while the second term, $\Lambda \langle u'w' \rangle$, indicates the conversion between the kinetic energy of the mean flow and that of the perturbation.

They will be denoted by:

$$\left.\begin{aligned} & g\alpha \langle T'w' \rangle \equiv \langle P, K' \rangle \\ \text{and} \quad & \\ & \Lambda \langle u'w' \rangle \equiv \langle K', \bar{K} \rangle \end{aligned}\right\} \qquad (7.2)$$

The last term of the right-hand side of (7.1) expresses dissipation due to viscous friction.

Our primary concern here is with the conversion processes between the kinetic energies of the mean flow and the perturbation which may change its features drastically with changes in the configuration of the perturbation. In the preceding sections, however, our discussion was restricted to the perturbations of $k_x^* = k_y^*$.

Now our discussion is extended to the perturbations of transverse and longitudinal modes. Figure 8 shows variations of vertical momentum transfer, $\langle U^* W^* \rangle$, and amplification rate σ^* with the ratio of the wavenumber in the y direction to that in the x direction, (k_y/k_x). Vertical momentum transfer is indicated by a solid line and the amplification rate by a broken line for different values of R_i. This is for the case of $R_a = 10^4$ and $k^* = 2$. A decreasing value of R_i results in a reduction of the amplification rate of a transverse perturbation for which $k_y/k_x \ll 1$, whereas little difference in the amplification rate of a longitudinal perturbation characterized by

$k_y/k_x \gg 1$ is found among the cases with different values of R_i. Since a small Richardson number corresponds to a large shear of the basic flow, it is evident that wind shear is effective in suppressing development of a transverse perturbation, but this is not the case for a longitudinal one. On the other hand, it is shown in Fig. 8 that vertical transfer of momentum is upward against the shear for smaller values of k_y/k_x, while it is downward for larger values of k_y/k_x. This indicates that a transverse perturbation ($k_y/k_x \ll 1$) results in transforming the kinetic energy of the perturbation to that of the mean flow through upward transfer of horizontal momentum against the shear. This is exactly what Asai (1964) concluded for a two-dimensional thermal convection in a vertical plane parallel to the mean flow with vertical shear for which k_y/k_x tends to zero. On the contrary, for a longitudinal perturbation, i.e., $k_y/k_x \gg 1$, the kinetic energy of the mean flow is converted to that of the perturbation through downward transfer of horizontal momentum.

Since the energy conversion processes are closely related to the structure of perturbation, each perturbation flow pattern may be expected to be different from the others. Figures 9(a) and (b) show contours of vertical velocity (solid lines) and the x component of horizontal velocity u (broken lines) in a vertical plane parallel to the basic flow for two cases: (a) is the case of $k_y/k_x = 0.1$ as an example of transverse perturbation, and (b) is the case of $k_y/k_x = 10$ as an

example of longitudinal perturbation. The Richardson number is fixed at unity and again $R_a = 10^4$ and $k^* = 2$ for both cases. The warm axis (thick dotted line) and the cold axis (thin dotted line) are inserted in Figs. 9(a) and (b) to form a general picture of the temperature field. The most remarkable feature is that the pattern of vertical velocity is in phase with that of the x component of velocity u for the transverse perturbation, whereas they are out of phase with each other for the longitudinal perturbation. These features agree with the vertical momentum transfer mentioned above.

Taking into account the distribution of the y component of velocity v not shown here, as well as w and u, we can draw a three-dimensional flow pattern of perturbation. Typical streamlines are schematically illustrated by thick solid lines with arrows in Figs. 10(a) and (b) for both the perturbations. Projections of the streamlines on the x-y plane, the x-z plane, and the y-z plane are also shown on the respective planes. The most significant difference between the cases can be found in their streamline pattern projected on the x-z plane. The streamline pattern tilts with height toward the shear for the transverse perturbation, as is expected from the result of the two-dimensional convection. The longitudinal perturbation tilts against the shear with height. The reason for this may be given by (2.12) which states that variation of w with respect to y, i.e., in the direction across the basic flow, twists the horizontal component of vorticity into the vertical component.

An inspection of Figs. 10(a) and (b) indicates that the kinetic energy of perturbation is produced by release of the potential energy contained in the unstably stratified fluid layer through upward heat transport regardless of the difference in the modes of perturbations. The energy flows associated with the perturbations of two modes are summarized in Fig. 11. Making use of the dimensionless quantities defined by (4.2), we can rewrite the energy transformation terms (7.2) as follows:

$$\left.\begin{aligned} &\langle P,K'\rangle = g\alpha\Gamma\nu\ \langle \Theta^* W^* \rangle \\ \text{and}\quad &\langle K',\bar{K}\rangle = \nu^2 h^{-2} \Lambda\ \langle U^* W^* \rangle \end{aligned}\right\} \qquad (7.3)$$

Then the ratio between the two terms is:

$$\begin{aligned} \frac{\langle K',\bar{K}\rangle}{\langle P,K'\rangle} &= \left(\frac{P_r}{R_a R_i}\right)^{\frac{1}{2}} \frac{\langle U^* W^* \rangle}{\langle \Theta^* W^* \rangle} \\ &= \frac{P_r R_e}{R_a} \frac{\langle U^* W^* \rangle}{\langle \Theta^* W^* \rangle} \end{aligned} \qquad (7.4)$$

If $\langle P,K'\rangle$ is normalized to unity in the examples of both transverse (a) and longitudinal perturbations (b), the values of $\langle K',\bar{K}\rangle$ become

$$\langle K', \bar{K} \rangle \doteq 0.23 \quad \text{for (a)}$$

and

$$\langle K', \bar{K} \rangle \doteq -0.75 \quad \text{for (b)}$$

for $R_a = 10^4$, $R_i = 1$ and $P_r = 7$. Reduction in the value of the Richardson number increases the magnitude of $\langle K', \bar{K} \rangle$. The conversion of potential energy to the kinetic energy is usually larger than that between the kinetic energies of the mean flow and the perturbation. The latter mechanism, however, plays an important role in determining a preferred mode of perturbation. Finally, it should be noted that the longitudinal perturbation, which is most favorable for development, inevitably results in a three-dimensional motion.

8. Conclusions

Three-dimensional features of perturbation in an unstably stratified plane Couette flow were investigated by solving numerically a system of linearized Boussinesq equations. Our main concern is with the dynamical structure and the associated energy conversion of the stationary unstable perturbation of the lowest mode in the vertical which is of primary importance for thermal convection.

Conversion between kinetic energy of the basic flow and that of the perturbation through vertical transfer of horizontal momentum takes place as well as conversion of potential energy to kinetic energy which results from upward heat transfer. In particular, vertical transfer of horizontal momentum depends crucially on the three-dimensional structure of the perturbation. It is upward against the shear of the basic flow and results

in transforming the kinetic energy of perturbation to that of the basic flow for a transverse perturbation. For a longitudinal perturbation, however, it is downward and transforms the kinetic energy of the basic flow to that of the perturbation. Thus it is suggested that a two-dimensional thermal convection in the vertical plane parallel to the basic flow will result in the vertical momentum transfer peculiar to a transverse perturbation which tends to intensify the shear of the basic flow. The longitudinal perturbation, which is most favorable for development, naturally leads to a three-dimensional motion.

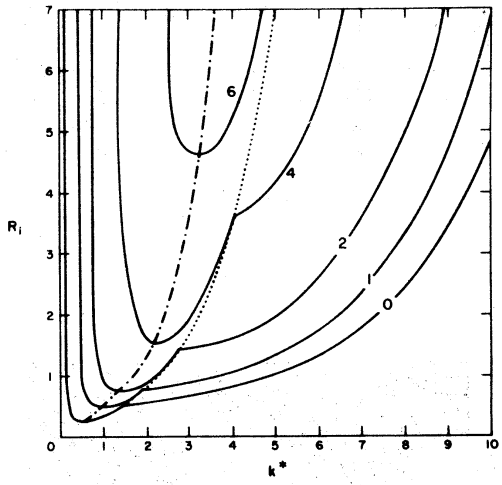

Fig. 2

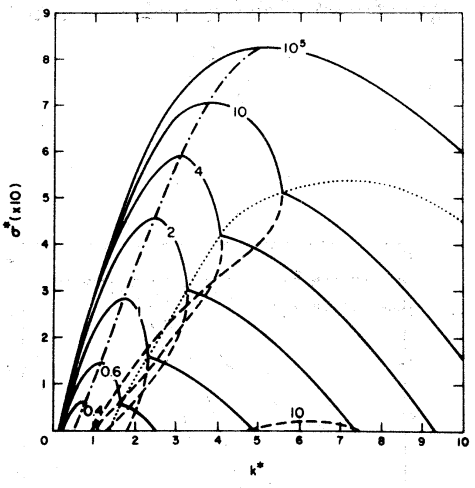

Fig. 3

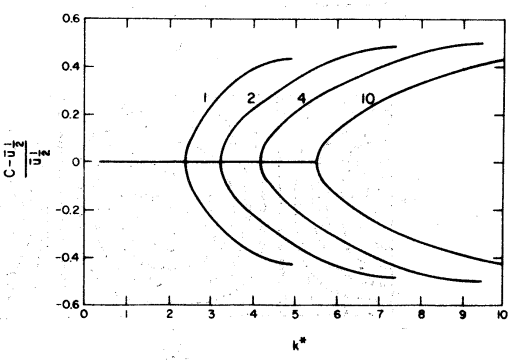

Fig. 4

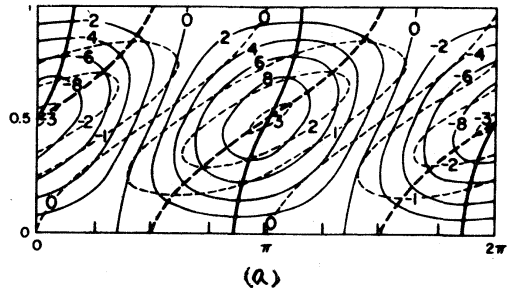

Fig. 5

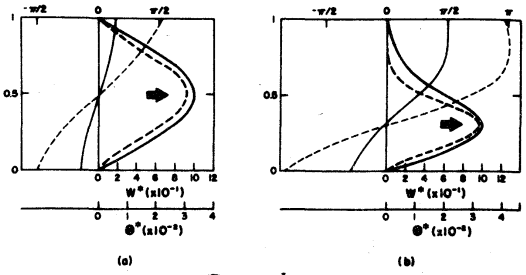

Fig. 6

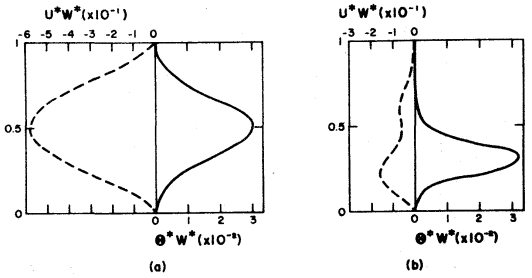

Fig. 7

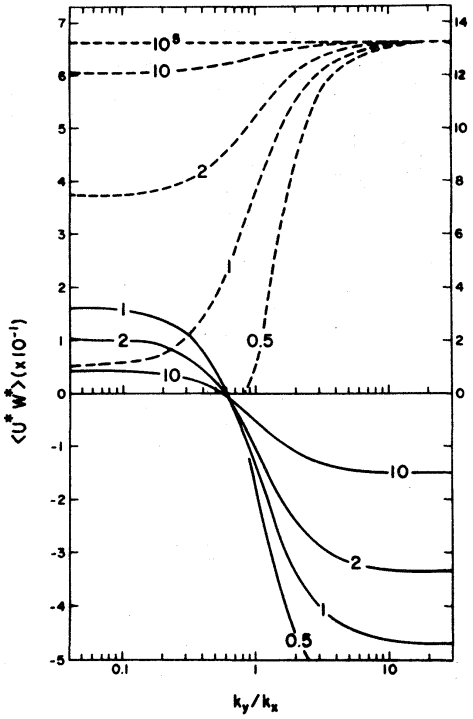

Fig. 8

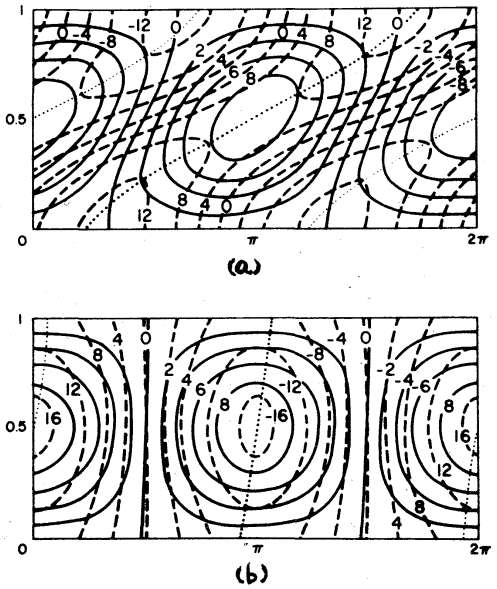

Fig. 9

REFERENCES

Asai, T., 1964: Cumulus convection in the atmosphere with vertical wind shear: Numerical experiment. J. Meteor. Soc. Japan, 42, 245-259.

_____ and I. Nakasuji, 1968: A numerical investigation of hydrodynamic instability of a shear flow in a thermally unstable fluid layer. Special Contributions, Geophys. Inst., Kyoto Univ., 8, 31-44.

Case, K. M., 1960: Stability of inviscid plane Couette flow. Phys. Fluids, 3, 143-148.

Chandra, K., 1938: Stability of fluids heated from below. Proc. Roy. Soc., A 164, 231-242.

Deardorff, J. W., 1965: Gravitational instability between horizontal plates with shear. Phys. Fluids, 8, 1027-1030.

Dyson, F. J., 1960: Stability of an idealized atmosphere, II, Zeros of the confluent hypergeometric function. Phys. Fluids, 3, 155-157.

Francis, J. G., 1961: The QR transformation: Part 1, Unitary analogue to the LR transformation. The Computer Journal, 4, 265-271.

_____, 1962: The QR transformation: Part 2. The Computer Journal, 4, 332, 345.

Gallagher, A. P. and A. McD. Mercer, 1965: On the behaviour of small disturbances in plane Couette flow with a temperature gradient. Proc. Roy. Soc. A 286, 117-128.

Graham, A., 1934: Shear patterns in an unstable layer of air. Phil. Trans. Roy. Soc., 232, A714, 285-296.

Ingersoll, A. P., 1966: Convective instabilities in plane Couette flow. Phys. Fluids, 9, 682-689.

Jeffreys, H., 1928: Some cases of instability in fluid motion. Proc. Roy. Soc., A118, 195-208.

Kuo, H. L., 1963: Perturbations of plane Couette flow in stratified fluid and origin of could streets. Phys. Fluids, 6, 195-211.

Lilly, D. K., 1969: Numerical simulation of two-dimensional turbulence. Submitted to Physics of Fluids.

Riis, E., 1962: The stability of Couette-flow in non-stratified and stratified viscous fluids. Geofys. Publ., 23, 1-37.

Taylor, G. I., 1931: Effect of variation in density on the stability of superposed streams of fluid. Proc. Roy. Soc., A132, 499-523.

Terada, T., 1928: Some experiments on periodic columnar formation of vortices caused by convection. Report Aeron. Res. Inst. Tokyo, 3, 1-46.

Wilkinson, J. H., 1965: The algebraic eigenvalue problem. Clarendon Press, Oxford, pp. 619-633.

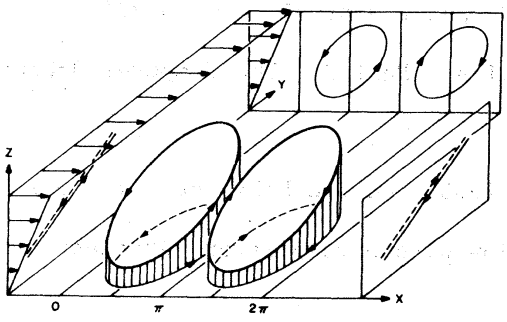

Fig. 10 (a)

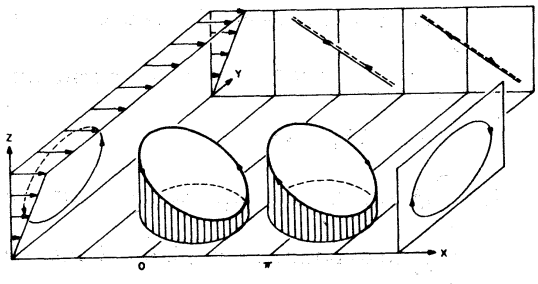

Fig. 10 (b)

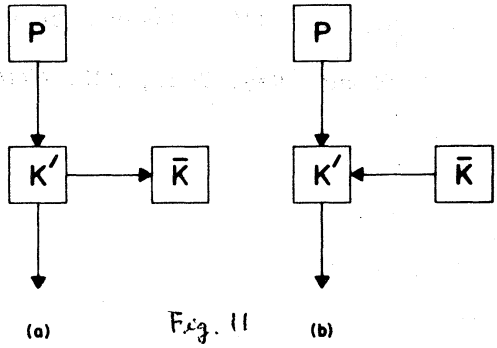

Fig. 11